Commun. Comput. Phys.
doi: 10.4208/cicp.151009.270910s

Vol. **9**, No. 5, pp. 1094-1105
May 2011

Roughness Effects on Continuous and Discrete Flows in Superhydrophobic Microchannels

Junfeng Zhang[1,*] and Daniel Y. Kwok[2]

[1] *School of Engineering, Laurentian University, Sudbury, Ontario, P3E 2C6, Canada.*
[2] *Nanoscale Technology and Engineering Laboratory, Department of Mechanical Engineering, Schulich School of Engineering, University of Calgary, Calgary, Alberta, T2N 1N4, Canada.*

Received 15 October 2009; Accepted (in revised version) 27 September 2010

Available online 24 December 2010

Abstract. The dynamic behaviors of continuous and discrete flows in superhydrophobic microchannels are investigated with a lattice Boltzmann model. Typical characters of the superhydrophobic phenomenon are well observed from our simulations, including air trapped in the surface microstructures, high contact angles, low contact angle hysteresis, and reduced friction to fluid motions. Increasing the roughness of a hydrophobic surface can produce a large flow rate through the channel due to the trapped air, implying less friction or large apparent slip. The apparent slip length appears to be independent to the channel width and could be considered as a surface property. For a moving droplet, its behavior is affected by the surface roughness from two aspects: the contact angle difference between its two ends and the surface-liquid interfacial friction. As a consequence, the resulting droplet velocity changes with the surface roughness as firstly decreasing and then increasing. Simulation results are also compared with experimental observations and better agreement has been obtained than that from other numerical method. The information from this study could be valuable for microfluidic systems.

PACS: 68.08.Bc, 05.70.Np, 83.50.Rp

Key words: Lattice Boltzmann method, interfacial slip, superhydrophobicity, solid-fluid interaction, roughness effect, microchannels.

1 Introduction

Superhydrophobic surfaces have recently been studied extensively for both scientific and engineering interests [10,20,21,37]. Most of these studies focus mainly on the contact angle behaviors. Due to the air trapped between the microstructures, the adhesion between

*Corresponding author. *Email addresses:* jzhang@laurentian.ca (J. Zhang), daniel.kwok@ucalgary.ca (D. Y. Kwok)

the surface and liquid is reduced and a droplet on such a surface exhibits high contact angles and low contact angle hysteresis (the difference between the advancing and receding angles). On the other side, Kim et al. [15] examined the sliding angles of droplets on rough hydrophobic surfaces and found that the friction from the solid surfaces to the liquid was greatly reduced. Richard and Quere [25] had also studied the drop moving behaviors on inclined surfaces. The drop was observed rolling down the superhydrophobic surface instead of sliding on hydrophilic surfaces. Takeda et al. [32] conducted other interesting experiments showing that a vertical electric field can lift a water droplet to jump up from a superhydrophobic surface.

Recently, several experiments have shown that the surface friction to continuous flows can also be reduced by employing superhydrophobic surfaces [5, 6, 9, 14, 18, 22]. These works demonstrated that the adhesion and friction between the liquid and superhydrophobic surfaces have been greatly reduced. However, contradictory to these experiments, theoretical and numerical investigations of this interesting and promising phenomenon are rare due to the difficulties from the geometric complexity, fluid dynamics, interfacial rheology, and multiple phases (liquid, vapor, and solid) involved; especially for discrete flows in spite of their attractiveness in digital microfluidics [8, 12].

Studying on fluid slip over a solid surface has long been an interesting subject since the pioneering work by Navier and Maxwell [41]. Recent measurements indeed indicate significant slip on solid surfaces [4,33,45]. Due to the difficulties in direct microscopic observation near the solid-fluid interface, numerical simulations, by means of molecular dynamics (MD) [7] and the lattice Boltzmann method (LBM) [27,41], have been employed to study the underlying mechanism and relationship between fluid slip and the properties of fluid and solid. In general, both experimental and simulation results show that there is a strong relationship between the magnitude of slip and the solid-fluid interaction: the weaker the interaction, the larger the contact angle and hence the slip. These studies are also usually conducted on smooth surfaces or continuous flows, and the roughness effects on continuous and discrete flow behaviors have not been well examined. Therefore, it is interesting and important to investigate the superhydrophobic effects on the fluid behaviors. A better understanding of the underlying physics will also provide guidance for the design and applications of superhydrophobic materials. In this paper, we present our LBM numerical studies on the continuous and discrete flow behaviors in rough and hydrophobic channels.

2 The mean-field free energy multiphase LBM model

Our simulations employ a recently proposed mean-field free energy LBM model for nonideal fluids for its physical representation of the solid-fluid interactions [44]. According to the mean-field version of the van der Waals theory, the total free energy F for a fluid system can be expressed as [26, 30, 40]

$$F=\int d\mathbf{r}\Big\{\psi[\rho(\mathbf{r})]+\frac{1}{2}\rho(\mathbf{r})\int d\mathbf{r}'\phi_{ff}(\mathbf{r}'-\mathbf{r})[\rho(\mathbf{r}')-\rho(\mathbf{r})]+\rho(\mathbf{r})V(\mathbf{r})\Big\}, \tag{2.1}$$

where $\psi(\rho)$ is a local free energy with respect to the bulk density ρ. The second term is a non-local term taking into account the free energy cost of variations in density; $\phi_{ff}(\mathbf{r}'-\mathbf{r})$ is the interaction potential between two fluid particles locating at $\mathbf{r}'$ and $\mathbf{r}$. This term can be reduced to that of a square-gradient approximation when the local density varies slightly [30, 34]. The third term represents contribution of an external potential energy $V(\mathbf{r})$ to the free energy F. Both integrations are taken over the entire space.

With this expression of free energy, we follow the procedures described by Yang et al. [35] and define a non-local pressure as

$$P(\mathbf{r})=\rho(\mathbf{r})\psi'[\rho(\mathbf{r})]-\psi[\rho(\mathbf{r})]+\frac{1}{2}\rho(\mathbf{r})\int d\mathbf{r}'\phi_{ff}(\mathbf{r}'-\mathbf{r})[\rho(\mathbf{r}')-\rho(\mathbf{r})]. \tag{2.2}$$

For a bulk fluid with uniform density, the non-local integral term disappears and Eq. (2.2) reverts to the equation of state of the fluid

$$P=\rho\psi'(\rho)-\psi(\rho). \tag{2.3}$$

Here, we briefly describe the implementation of these results into a LBM algorithm. In general, after discretization in time and space, the lattice Boltzmann equation (LBE) with a Bhatnagar-Gross-Kooky (BGK) collision term can be written as [2,38]

$$f_i(\mathbf{x}+\mathbf{e}_i,t+1)-f_i(\mathbf{x},t)=-\frac{1}{\tau}\left[f_i(\mathbf{x},t)-f_i^{eq}(\mathbf{x},t)\right], \tag{2.4}$$

where the distribution function $f_i(\mathbf{x},t)$ denotes particle population moving in the direction of $\mathbf{e}_i$ at a lattice site $\mathbf{x}$ with a time step t; τ is a relaxation time and $f_i^{eq}(\mathbf{x},t)$ is the prescribed equilibrium distribution function. The macroscopic density ρ and velocity $\mathbf{u}$ can be calculated from the distribution function f_i given by

$$\rho=\sum_i f_i, \tag{2.5a}$$

$$\rho\mathbf{u}=\sum_i f_i\mathbf{e}_i. \tag{2.5b}$$

However, if an external force $\mathbf{F}(\mathbf{x},t)$ exists, we can modify Eq. (2.5b) to reflect the momentum change as

$$\rho\mathbf{u}=\sum_i f_i\mathbf{e}_i+\tau\mathbf{F} \tag{2.6}$$

and employ the $\mathbf{u}$ here to calculate the equilibrium distribution function f_i^{eq} in Eq. (3.3) [1, 28]. Redefining the fluid momentum $\rho\mathbf{v}$ to be an average of the momentum before collision $\sum_i f_i\mathbf{e}_i$ and that after collision $(\rho\mathbf{u}+\mathbf{F})$ yields

$$\rho\mathbf{v}=\sum_i f_i\mathbf{e}_i+\frac{1}{2}\mathbf{F}. \tag{2.7}$$

Following the Chapman-Enskog procedure, a Navier-Stokes equation with the equation of state

$$P=\frac{c^2(1-d_0)}{D}\rho+\Phi \tag{2.8}$$

can be obtained, where Φ is the potential field related to $\mathbf{F}$ by

$$\mathbf{F}(\mathbf{x},t)=-\nabla\Phi(\mathbf{x},t). \tag{2.9}$$

In order to obtain the Navier-Stokes equation with a pressure term similar to that given by Eq. (2.2), we set an artificial Φ as follows

$$\Phi(\mathbf{x},t)=\rho(\mathbf{x})\psi'[\rho(\mathbf{x})]-\psi[\rho(\mathbf{x})]+\frac{1}{2}\rho(\mathbf{x})\int d\mathbf{x}'\phi_{ff}(\mathbf{x}'-\mathbf{x})[\rho(\mathbf{x}')-\rho(\mathbf{x})]-\frac{c^2(1-d_0)}{D}\rho(\mathbf{x}). \tag{2.10}$$

The above equations set up a complete LBM scheme with the mean-field free energy function implemented. Simulations have demonstrated its realistic representation of the solid-fluid interactions [41,43].

3 Simulation set-up and numerical implementation

Following [31,44], we employ a van der Waals fluid model to express the free-energy of bulk fluid:

$$\psi(\rho)=\rho kT\ln\frac{\rho}{1-b\rho}-a\rho^2, \tag{3.1}$$

where a and b are the van der Waals constants; k is the Boltzmann constant and T is the absolute temperature. In this study, we selected $a=9/49$, $b=2/21$ and the scaled temperature $kT=0.52$. The choice of this set of parameters was also based on previous studies [31,44].

In this work, a D2Q9 (two dimensions and nine lattice velocities) lattice structure (Fig. 1(a)) was employed. The nine discrete lattice velocities are expressed as

$$\mathbf{e}_0=\mathbf{0}, \tag{3.2a}$$

$$\mathbf{e}_i=\Big(\cos\frac{i-1}{2}\pi,\sin\frac{i-1}{2}\pi\Big), \qquad i=1-4, \tag{3.2b}$$

$$\mathbf{e}_i=\sqrt{2}\Big(\cos\frac{2i-9}{4}\pi,\sin\frac{2i-9}{4}\pi\Big), \quad i=5-8, \tag{3.2c}$$

and the equilibrium distribution f_i^{eq} is given as [23,36]:

$$f_0^{eq}=\rho\Big(1-\frac{2}{3}\mathbf{u}^2\Big), \tag{3.3a}$$

$$f_i^{eq}=\rho\Big[\frac{1}{9}+\frac{1}{3}\mathbf{e}_i\cdot\mathbf{u}+\frac{1}{2}(\mathbf{e}_i\cdot\mathbf{u})^2-\frac{1}{6}\mathbf{u}^2\Big], \qquad i=1-4, \tag{3.3b}$$

$$f_i^{eq}=\rho\Big[\frac{1}{36}+\frac{1}{12}\mathbf{e}_i\cdot\mathbf{u}+\frac{1}{8}(\mathbf{e}_i\cdot\mathbf{u})^2-\frac{1}{24}\mathbf{u}^2\Big], \quad i=5-8. \tag{3.3c}$$

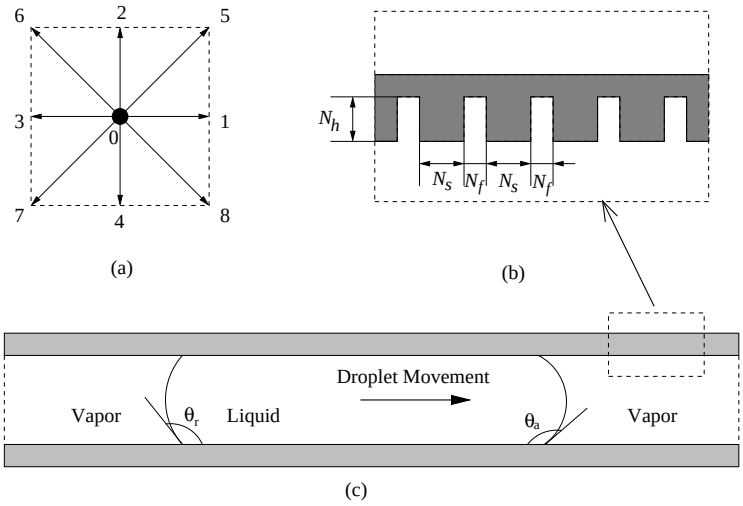

Figure 1: Schematics of the D2Q9 lattice structure (a), the rough surface model (b), and the simulation setup for droplet movement in a rough channel (c) employed in this study.

By considering only interactions between neighboring lattice nodes as done in previous studies [28, 31, 42], the fluid-fluid interaction potential ϕ_{ff} can be reduced to a single number K

$$\phi_{ff}(\mathbf{x}'-\mathbf{x}) = \begin{cases} K, & |\mathbf{x}'-\mathbf{x}|=1, \\ K/4, & |\mathbf{x}'-\mathbf{x}|=\sqrt{2}, \\ 0, & \text{otherwise}, \end{cases} \tag{3.4}$$

where K represents the interaction strength among fluid particles; and the non-local integral term can be replaced by a summation over the neighbors of a site $\mathbf{x}$. In this work, K was set to -0.02; a negative value implies an attraction between two fluid particles and its magnitude affects the liquid-vapor interfacial tension. Similarly, the solid-fluid interactions was implemented as an attractive force between a solid ($\mathbf{x}_s$) and a liquid ($\mathbf{x}_f$) site as

$$\mathbf{F_s} = \begin{cases} K_w\rho(\mathbf{x}_f)(\mathbf{x}_s-\mathbf{x}_f), & |\mathbf{x}_s-\mathbf{x}_f|=1, \\ K_w\rho(\mathbf{x}_f)(\mathbf{x}_s-\mathbf{x}_f)/4\sqrt{2}, & |\mathbf{x}_s-\mathbf{x}_f|=\sqrt{2}, \\ 0, & \text{otherwise}. \end{cases} \tag{3.5}$$

The coefficient K_w is positive for attractive forces and can be adjusted to obtain different wettability (contact angles). The larger the K_w, the stronger the solid-liquid **attractions** and hence the solid-liquid work of adhesion, resulting in a smaller contact angle. Here K_w was selected as 0.07 to produce a relatively larger contact angle of 127.8° on a flat surface [43] to mimic a hydrophobic surface (e.g., a Teflon surface).

A rough surface was simply modeled with solid asperities separated by void spaces, and various roughness can be obtained by adjusting the relative widths of the solid asperities N_s and void gaps N_f (Fig. 1(b)). Such a model also represents well the superhydrophobic surfaces utilized in several experiments [6, 9]. Similar to that in [9], we define

the ratio $r=N_f/(N_s+N_f)$ as a measure of the surface roughness. $r=0$ corresponds a flat surface and a larger r represents a more rough surface. For simplicity, the sum N_s+N_f was held constant 30 lattice units throughout this study. To study the contact angle and droplet movement in such rough channels, a segment of the channel was filled with liquid and the rest with vapor (Fig. 1(c)). The general no-slip bounce-back scheme was employed for the solid-fluid interfaces and periodic boundary conditions were applied in the horizontal direction. Fluid motion was induced by means of a body force **g** along the channel.

4 Results and discussion

Firstly, continuous flows driven by a body force were simulated in the above modeled channels. Fig. 2 shows (a) the liquid/vapor configuration and (b) the streamwise velocity profiles across the channel with $r=0.67$. Initially, the coexistence liquid and vapor densities, 1.58 and 5.68, were assigned to the gap regions between solid blocks and the channel central region, respectively. During the calculation, the fluid density at the central region is maintained at the coexistence liquid density.

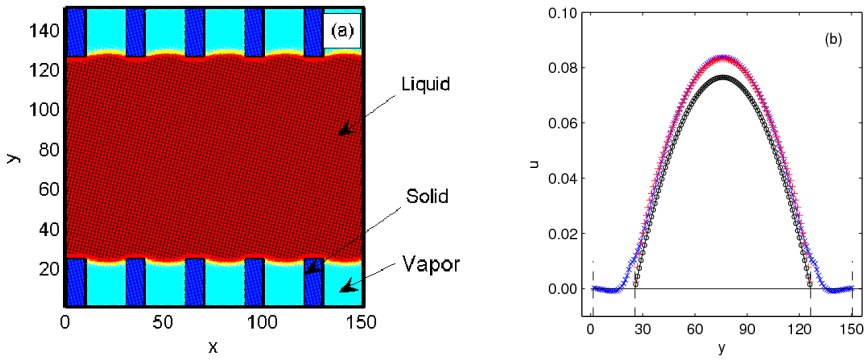

(a) (b)

Figure 2: (color online) (a) The liquid-vapor configuration (red for liquid, cyan for vapor, and blue for solid) and (b) velocity profiles in a channel with roughness $r=0.67$ and height $2h=101$. The color symbols represent the results from the mean-field LBM at the asperity center ($x=5$, red $+$) and the gap center ($x=20$, blue $\times$). Profiles from a general LBM simulation (black $\circ$) and fluid mechanics (black solid line) are also displayed for comparison. The short vertical dashed lines indicate the solid-fluid interface positions: $y=1.5$ (gap bottom), 25.5 (asperity top), 126.5 (asperity top), and 150.5 (gap bottom).

It can be seen that, due to the hydrophobic nature of the surface, the Laplace pressure prevents the liquid from penetrating into the gaps and vapor is trapped there. This is the most important character of superhydrophobic surfaces and our simulations captured it well (Fig. 2(a)). In Fig. 2(b), velocities from our mean-field free energy LBM simulations at two different locations, the asperity center ($x=5$, red $+$) and the gap center ($x=20$, blue $\times$), in the rough channel are compared with those from a general LBM [23] (black $\circ$) and fluid mechanics (black solid line) in a smooth channel of a same height. For all

these profiles from LBM, the no-slip solid-fluid boundary condition on the solid surface is well satisfied. No surprising, the results from the general LBM and fluid mechanics agree each other well, since the general LBM is in fact a Navier-Stokes solver in bulk fluid domain [29]. However, with incorporating the effects from the surface roughness, hydrophobicity, and trapped vapor, the velocity from our mean-field LBM simulation is larger than those without considering these important factors. This results in a larger flow rate. From a macroscopic point of view, such a larger flow rate can be interpreted as less friction to the fluid motion from the channel surfaces, or as an apparent (or effective) interfacial slip over the surface.

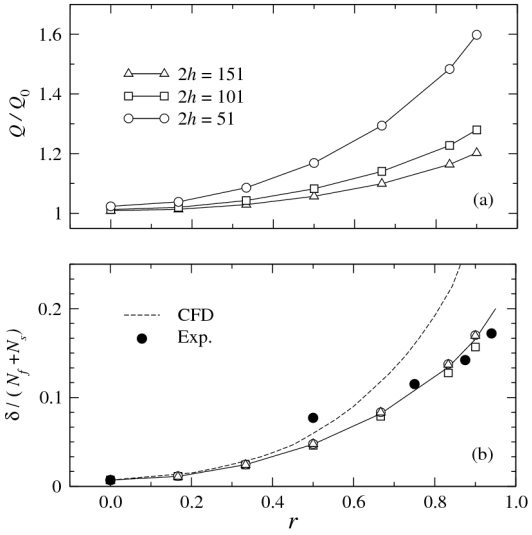

Figure 3: (a) The normalized flow rate Q/Q_0 and (b) the apparent slip length δ in channels with different roughness r and channel height $2h$. Also displayed in (b) are the experimental (filled circles) and other CFD numerical (dashed line) results from [9] for comparison.

For the convenience of further quantitative analysis, the apparent slip is characterized by a slip length δ. According to the Navier hypothesis for fluid slip, the slip length δ is related to the flow rate Q induced by a body force g in a channel with height $2h$ by [4]

$$\delta = \frac{\nu Q}{2h^2 g} - \frac{h}{3}, \tag{4.1}$$

where ν is the fluid kinematic viscosity. Fig. 3 displays (a) the normalized flow rate Q/Q_0 ($Q_0 = 2h^3 g/3\nu$ is the flow rate in a smooth channel from fluid mechanics) and (b) the apparent slip length δ in channels with different surface roughness and channel heights. We noticed that, even in smooth hydrophobic channels ($r = 0$), apparent slip ($Q/Q_0 > 1$ and $\delta > 0$) can be observed due to the surface hydrophobicity [41]. Both the normalized flow rate and the slip length are increasing with the surface roughness r, in good agreement to previous studies [9, 16]. These results show that the friction to the fluid motion from the

channel surface is indeed reduced greatly by increasing the roughness of a hydrophobic surface to trap more vapor/air between the surface microstructures. On the other hand, we also find that, for channels with same surface roughness, Q/Q_0 is larger for smaller channels, implying that such surface effects deserve more attention for small-scale systems. However, the apparent slip length seems not influenced by the channel size much and can be considered as a constant property for a certain surface. Similar behaviors have been observed in previous experiments [6,22]. Also in Fig. 3(b), we compared the apparent slip length results from our LBM simulations with recent experimental data and numerical predictions from a traditional computational fluid dynamics (CFD) method [9]. Clearly, our LBM results match the experimental observation very well, while the CFD method generally overestimated the slip magnitude. The deviation could be due the over simplified treatment by neglecting the meniscus penetration into the cavity [9]. Actually the surface wettability (contact angle) effect, which indeed plays a determinant role in the flow slip phenomenon as demonstrated experimentally [6], was not incorporated at all in such a CFD model.

Multiphase flows with droplets/bubbles are commonly found in recent digital microfluidic systems [3, 8, 12]. By enclosing a liquid column and filling the rest space in the channel with vapor, the discrete flow behaviors and droplet movement can be studied [42, 43]. Unlike those on a smooth surface, the stick-jump-slip contact point movement and contact angle variation had been observed as the contact point moves over a rough surface [43]. Such movement and variation had also been reported from experiments [11,24]. In Fig. 4(a), we plotted the averaged advancing (filled circles) and receding (open circles) angles verse roughness r under a driving body force g=1×10^{-7}. At first, the advancing angle increases much faster than the receding angle with roughness r. However, after a moderate value ($r\sim0.5$ here), the increase of advancing angle slows down and finally decreases slightly at high roughness; and hence the contact angle hysteresis reaches its maximum value at the moderate roughness and becomes smaller at high roughness. These results are in qualitative agreement with experimental observations of the high contact angles and low hysteresis on superhydrophobic surfaces [13]. We would also like to point out that, even for such a simple surface model, the contact angle displays a quite complex fashion; and hence caution should be executed when interpreting experimental results on real surfaces [39].

The corresponding droplet velocity is also shown in Fig. 4(b). It is interesting to find that the velocity change exhibits two regimes with the roughness r: decreasing at first and, after a moderate roughness ($r\sim0.5$ here), increasing with the roughness r. Such a behavior is qualitatively understandable by considering the force balance between the driving force and resistances to the moving droplet. The driving force here is the body force g, which is constant for all surfaces with different r. However, the resistances consist of two parts: the friction from the channel surfaces and the unbalanced capillary force from the contact angle difference at the two liquid ends [17]; and they both are changing with surface roughness r. For the first part, the friction from the droplet-channel contact surface decreases with roughness r due to larger portion of trapped vapor in the

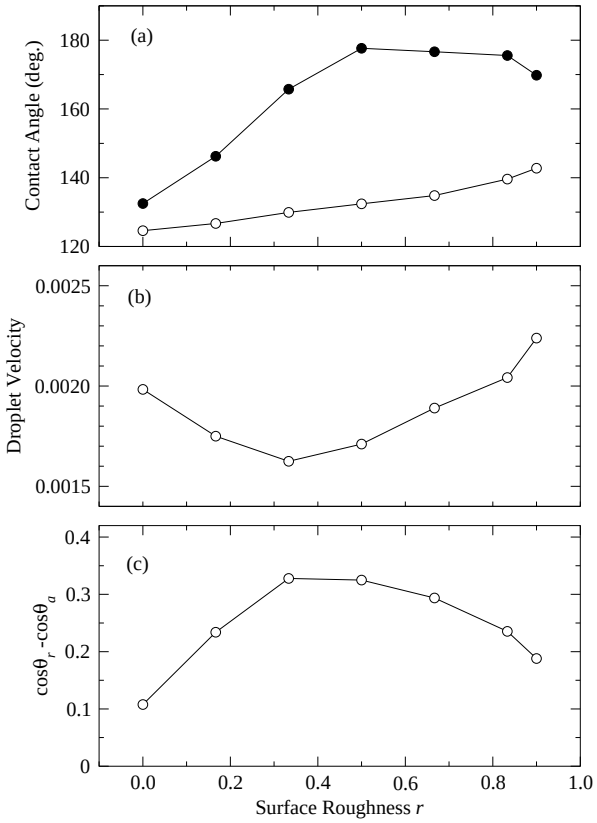

Figure 4: (a) The advancing θ_a (filled circles) and receding θ_r (open circles) contact angles, (b) droplet velocity, and (c) cos-difference between the advancing and receding contact angles on different rough surfaces.

void space, as indicated in Fig. 3. However, the contact angle difference and hence the unbalanced capillary force F_σ

$$F_\sigma = 2\sigma(\cos\theta_r - \cos\theta_a) \tag{4.2}$$

(where σ is the interfacial tension and θ_r and θ_a are, respectively, the advancing and receding angles) increases in the low r regime and decreases in the high r regime (see Fig. 4(c)). Therefore, in the low r regime, the increasing contact angle difference dominates the droplet movement, resulting a lower droplet velocity. As r increases to a higher value ($r > 0.5$), the contact angle difference decreases slightly, while the surface friction also becomes smaller. Together these reduced resistances produce higher velocity on superhydrophobic surfaces. The experimental study by Kim et al. [15] confirmed the high roughness regime with small sliding angle on superhydrophobic surfaces. With the fast development of fabrication technologies, surfaces with very high roughness are readily available [14, 15, 19]. From the changing trends displayed in Fig. 4, it is reasonable to anticipate further smaller contact angle hysteresis and larger droplet velocities on more rough surfaces.

5 Summary

We have numerically investigated the continuous and discrete flow behaviors in superhydrophobic channels by means of a mean-field free energy LBM model. Principle characters of superhydrophobic surfaces, including vapor/air trapped between rough microstructures, high contact angles, low contact angle difference, and low surface friction to liquid motion, are all well observed. The continuous flow in a superhydrophobic channel exhibits larger velocity compared to that in a smooth one due to the trapped vapor, resulting in a larger flow rate, less friction or apparent slip over the channel surfaces. According to the simulation results in channels, the apparent slip length is independent to the channel size and can be considered as a surface property, in consistence to experimental observations. With a physical representation of the surface wettability effect, our model provides a better description of the friction reduction and apparent slip in superhydrophobic channels than a traditional CFD method when compared to experimental data. For discrete flows, the droplet movement on a rough and hydrophobic surface is affected by the surface roughness through two aspects: the contact angle difference and the surface friction; and the droplet velocity hence displays two regimes changing with the roughness: firstly decreasing and then increasing after a moderate roughness. These findings could be valuable for the design and applications of superhydrophobic materials in microfluidic systems and deserve further examination.

Acknowledgments

This work was supported by the Natural Sciences and Engineering Research Council of Canada (NSERC) and the Laurentian University Research Fund to JZ. The authors also thank the anonymous reviewer for his/her critical comments and constructive suggestions.

References

[1] J. M. Buick, Ph.D. Thesis: Lattice Boltzmann Methods in Interfacial Wave Modelling, The University of Edinburgh, U.K., 1997.
[2] S. Chen and G. D. Doolen, Lattice Boltzmann method for fluid flows, Annu. Rev. Fluid. Mech., 30 (1998), 329–364.
[3] S. K. Cho, H. Moon, and C. J. Kim, Creating, transporting, cutting, and merging liquid droplets by electrowetting-based actuation for digital microfluidic circuits, J. MEMS., 12(1) (2002), 70–80.
[4] C. Choi, A. Westin, and K. Breuer, Apparent slip flows in hydrophilic and hydrophobic microchannels, Phys. Fluids, 5 (2003), 2897–2902.
[5] C.-H. Choi and C.-J. Kim, Large slip of aqueous liquid flow over a nanoengineered superhydrophobic surface, Phys. Rev. Lett., 96 (2006), 066001.
[6] C.-H. Choi, U. Ulmanella, J. Kim, C.-M. Ho, and C.-J. Kim, Effective slip and friction reduction in nanograted superhydrophobic microchannels, Phys. Fluids, 18 (2006), 087105.

[7] M. Cieplak, J. Koplik, and J. R. Banavar, Boundary conditions at a fluid-solid interface, Phys. Rev. Lett., 86 (2001), 803–806.
[8] A. Darhuber and S. Troian, Principles of microfluidic actuation by modulation of surface stresses, Ann. Rev. Fluid. Mech., 37 (2005), 425–455.
[9] J. Davies, D. Maynes, B. W. Webb, and B. Woolford, Laminar flow in a microchannel with superhydrophobic walls exhibiting transverse ribs, Phys. Fluids, 18 (2006), 087110.
[10] H. Erbil, A. Demirel, Y. Avci, and Q. Mert, Transformation of a simple plastic into a superhydrophobic surface, Science, 299(5611) (2003), 1377–1380.
[11] M. Gleiche, L. Chi, E. Gedig, and H. Fuchs, Anisotropic contact-angle hysteresis of chemically nanostructured surfaces, Chemphyschem., 2(3) (2001), 187.
[12] S. Haeberle and R. Zengerle, Microfluidic platforms for lab-on-a-chip applications, Lab. Chip, 7 (2007), 1094–1110.
[13] R. E. Johnson, Jr. and R. H. Dettre, Contact angle hysteresis: contact angle measurements on rough surfaces, Adv. Chem. Ser., 43 (1963), 112–144.
[14] P. Joseph, C. Cottin-Bizonne, J.-M. Benoit, C. Ybert, C. Journet, P. Tabeling, and L. Bocquet, Slippage of water past superhydrophobic carbon nanotube forests in microchannels, Phys. Rev. Lett., 97 (2006), 156104.
[15] J. Kim and C. J. Kim, Nanostructured surfaces for dramatic reduction of flow resistance in droplet-based microfluidics, Proc. IEEE Int. Conf. MEMS., (2002), 479–482.
[16] E. Lauga and H. Stone, Effective slip in pressure-driven Stokes flow, J. Fluid. Mech., 489 (2003), 55.
[17] S.-W. Lee, D. Y. Kwok, and P. E. Laibinis, Chemical influences on adsorption-mediated self-propelled drop movement, Phys. Rev. E, 65 (2002), 051602.
[18] D. Maynes, K. Jeffs, B. Woolford, and B. W. Webb, Laminar flow in a microchannel with hydrophobic surface patterned microribs oriented parallel to the flow direction, Phys. Fluids, 19 (2007), 093603.
[19] M. Miwa, A. Nakajima, A. Fujishima, K. Hashimoto, and T. Watanabe, Effects of the surface roughness on sliding angles of water droplets on superhydrophobic surfaces, Langmuir, 16 (2000), 5754–5760.
[20] A. Nakajima, K. Hashimoto, and T. Watanabe, Recent studies on super-hydrophobic films, Monatshefte fur Chemie, 132 (2001), 31–41.
[21] R. Narhe and D. Beysens, Nucleation and growth on a superhydrophobic grooved surface, Phys. Rev. Lett., 93(7) (2004), 076103.
[22] J. Ou and J. P. Rothstein, Direct velocity measurements of the flow past drag-reducing ultrahydrophobic surfaces, Phys. Fluids, 17 (2005), 103606.
[23] Y. H. Qian, D. d'Humieres, and P. Lallemand, Lattice BGK models for Navier-Stokes equation, Europhys. Lett., 17 (1992), 479–484.
[24] M. Fabrettoand J. Ralston and R. Sedev, Contact angle measurements using the Wilhelmy balance for asymmetrically treated samples, J. Adhesion. Sci. Tech., 18(1) (2004), 29–37.
[25] D. Richard and D. Quere, Viscous drops rolling on a tilted non-wettable solid, Europhys. Lett., 48 (3) (1999), 286–291.
[26] J. Rowlinson and B. Widom, Molecular Theory of Capilary, Claredon, Oxford, 1982.
[27] M. Sbragaglia, R. Benzi, L. Biferale, S. Succi, and F. Toschi, Surface roughness-hydrophobicity coupling in microchannel and nanochannel flows, Phys. Rev. Lett., 97 (2006), 204503.
[28] X. Shan and H. Chen, Simulation of nonideal gases and liquid-gas phase-transitions by the lattice Boltzmann equation, Phys. Rev. E, 49 (1994), 2941–2948.

[29] S. Succi, Mesoscopic modeling of slip motion at fluid-solid interfaces with heterogeneous catalysis, Phys. Rev. Lett., 89 (2002), 064502.
[30] D. E. Sullivan, Surface tension and contact angle of a liquid–solid interface, J. Chem. Phys., 74(4) (1981), 2604–2615.
[31] M. R. Swift, W. R. Osborn, and J. M. Yeomans, Lattice Boltzmann simulation of nonideal fluids, Phys. Rev. Lett., 75 (1995), 830–833.
[32] K. Takeda, A. Nakajima, K. Hashimoto, and T. Watanabe, Jump of water droplet from a super-hydrophobic film by vertical electric field, Surface. Sci., 519 (2002), L589–L592.
[33] D. Tretheway and C. Meinhart, Apparent fluid slip at hydrophobic microchannel walls, Phys. Fluids, 14 (2002), L9–L12.
[34] B. Widom, Structure of interfaces from uniformity of the chemical potential, J. Stat. Phys., 19 (1978), 563.
[35] A. J. M. Yang, P. D. Fleming, and J. H. Gibbs, Molecular theory of surface tension, J. Chem. Phys., 64(9) (1976), 3732.
[36] Z. L. Yang, T. N. Dinh, R. R. Nourgaliev, and B. R. Sehgal, Numerical investigation of bubble coalescence characteristics under nucleate boiling condition by a lattice Boltzmann model, Int. J. Therm. Sci., 39 (2000), 1–17.
[37] L. Zhai, F. Cebeci, R. Cohen, and M. Rubner, Stable superhydrophobic coatings from polyelectrolyte multilayers, Nano. Lett., 4(7) (2004), 1349–1353.
[38] J. Zhang, Lattice Boltzmann method for microfluidics: models and applications, Microfluid. Nanofluid., DOI:10.1007/s10404–010–0624–1 (in press), 2010.
[39] J. Zhang, K. Grandke, and D. Y. Kwok, Comment on "surface characterization of hydrosilylated polypropylene: contact angle measurement and atomic force microscopy", Langmuir, 19(24) (2003), 10457–10458.
[40] J. Zhang and D. Y. Kwok, Calculation of solid-liquid work of adhesion patterns from combining rules for intermolecular potentials, J. Phys. Chem. B, 106 (2002), 12594.
[41] J. Zhang and D. Y. Kwok, Apparent slip over a solid-liquid interface with a no-slip boundary condition, Phys. Rev. E, 70 (2004), 056701.
[42] J. Zhang and D. Y. Kwok, Lattice Boltzmann study on the contact angle and contact line dynamics of liquid-vapor interfaces, Langmuir, 20 (2004), 8137–8141.
[43] J. Zhang and D. Y. Kwok, Contact line and contact angle dynamics in superhydrophobic channels, Langmuir, 22(11) (2006), 4998–5004.
[44] J. Zhang, B. Li, and D. Y. Kwok, Mean-field free-energy approach to the lattice Boltzmann method for liquid-vapor and solid-fluid interfaces, Phys. Rev. E, 69 (2004), 032602.
[45] Y. Zhu and S. Granick, Limits of the hydrodynamic no-slip boundary condition, Phys. Rev. Lett., 88 (2002), 106102.